The complete (3-D) surface displacement field in the epicentral area of the 1999 M_w7.1 Hector Mine earthquake, California, from space geodetic observations

Yuri Fialko,[1] Mark Simons

Seismological Laboratory, California Institute of Technology, Pasadena, California

Duncan Agnew

Institute of Geophysics and Planetary Physics, Scripps Institution of Oceanography, University of California San Diego, La Jolla, California.

Abstract. We use Interferometric Synthetic Aperture Radar (InSAR) data to derive continuous maps for three orthogonal components of the co-seismic surface displacement field due to the 1999 M_w7.1 Hector Mine earthquake in southern California. Vertical and horizontal displacements are both predominantly antisymmetric with respect to the fault plane, consistent with predictions of linear elastic models of deformation for a strike-slip fault. Some deviations from symmetry apparent in the surface displacement data may result from complexity in the fault geometry.

Introduction

The October 16, 1999 M_w7.1 Hector Mine earthquake is the best geodetically documented major strike-slip earthquake to date. The earthquake occurred in an arid sparsely vegetated remote area of the Mojave Desert, southern California, that is ideally suited for studies using Interferometric Synthetic Aperture Radar (InSAR). Pre- and post-seismic radar images of the earthquake area are available from both ascending and descending orbits, with acquisitions from the descending orbit separated by only one month. Because the current generation of InSAR satellites has only two radar look directions, previous InSAR studies of deformation due to earthquakes were generally limited to one or two components of the surface displacement field (projected onto the satellite line of sight) [e.g., *Massonnet et al.*, 1993; *Fujiwara et al.*, 2000]. We show that the InSAR data for the Hector Mine earthquake is sufficient to infer a complete three-dimensional (3-D) co-seismic surface displacement field by combining the radar amplitude and phase measurements. The Hector Mine earthquake occurred within a dense Global Positioning System (GPS) network, which allows us to validate the InSAR-derived results with the independent GPS data. As we demonstrate below, the co-seismic surface displacement field inferred from the space geodetic observations makes possible detailed inferences about the amount and distribution of slip on the earthquake fault, the extent of

off-fault deformation, and the overall mechanical properties of the upper Earth's crust.

Data analysis

The Hector Mine earthquake ruptured 40 to 50 km of the North-West trending right-lateral Bullion and Lavic Lake faults that are part of the Eastern California Shear Zone (ECSZ) [*USGS et al.*, 2000]. This area was imaged by the European Space Agency satellites ERS-1 and 2. The InSAR data used in this study consist of one interferometric pair from a descending orbit (track 127, frames 2907 and 2925) spanning a time interval of one month before, and four days after the earthquake (1999/10/20-1999/09/15), and one pair from an ascending orbit (track 77, frames 675 and 693) spanning a time interval of approximately four years before, and one months after the earthquake (1999/11/21-1995/11/12). The radar phase coherence is quite high even for the 4-year pair, presumably due to low levels of precipitation and sparse vegetation in the Mojave Desert. Such high phase coherence is not unusual for California, where correlation of the ERS radar images may be maintained over time periods as long as 7 years [e.g., *Fialko and Simons*, 2000]. Inspection of an independent ascending interferogram spanning a time interval from four years to two months before the earthquake (1999/08/08-1995/05/20) indicates that there has been no significant (more than a few centimeters) deformation in the rupture area of the Hector Mine earthquake between 1995 and 1999, so that the ascending interferogram covering the earthquake date is likely dominated by the co-seismic signal. The GPS data used in this study include measurements from one continuous, and 48 survey-mode GPS stations within 50 km from the earthquake epicenter.

We use a mosaic of 224 USGS digital elevation maps with 30 m postings to remove the effects of topography from interferometric images. The interferometric pairs have large heights of ambiguity (about 200 and 500 m for the ascending and descending orbits, respectively), implying that their sensitivity to digital elevation errors should be small. The interferograms have been processed using the Jet Propulsion Laboratory/Caltech repeat orbit interferometry package ROI_PAC. Figures 1a-b show interferograms from the ascending and descending orbits, respectively. Color fringes denote displacements along the satellite's line of sight (LOS) direction, and white areas mark decorrelated regions; as one

---

[1]Now at Institute of Geophysics and Planetary Physics, UCSD, La Jolla, California.
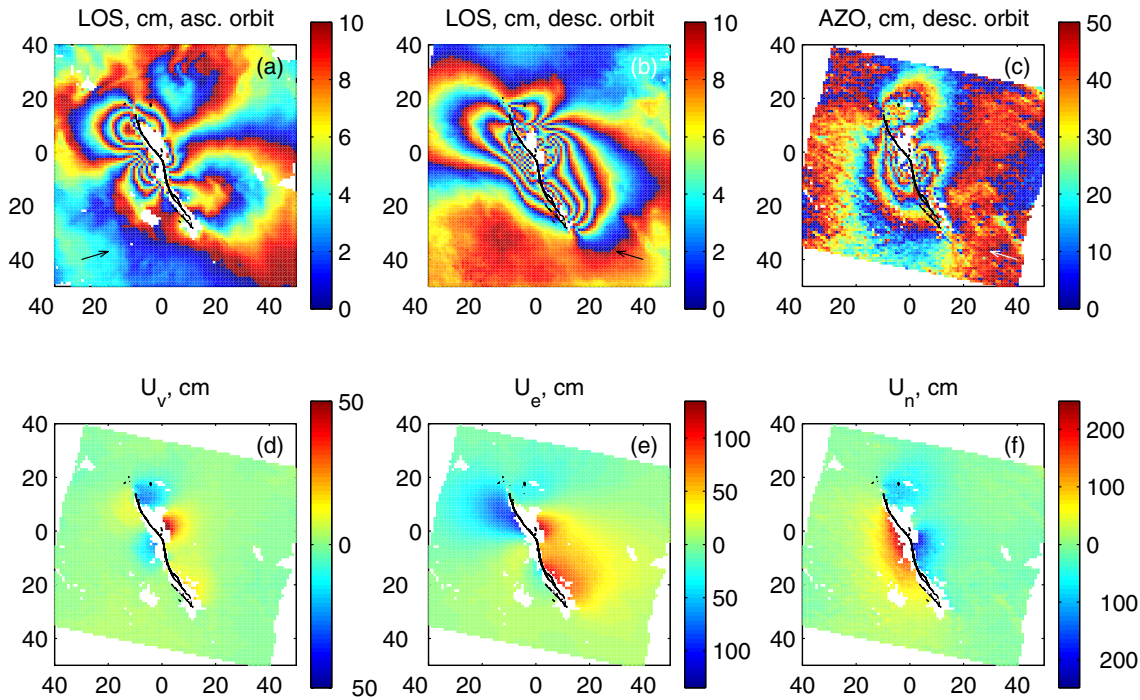
Figure 1. (a) Interferogram for the time period 99/11/21-95/11/12, ascending orbit. (b) Interferogram for the time period 99/10/20-99/09/15, descending orbit. (c) Azimuthal offsets, descending orbit. Arrows show the look direction from the satellite to the ground. (d)-(f) Up, East, and North components of the surface displacement field, respectively, obtained from the InSAR data. In all figures coordinates are in kilometers, with origin corresponding to the epicenter of the Hector Mine earthquake (116.27°W, 34.595°N). Black wavy lines denote the geologically mapped surface rupture (data courtesy of K. Kendricks, USGS).
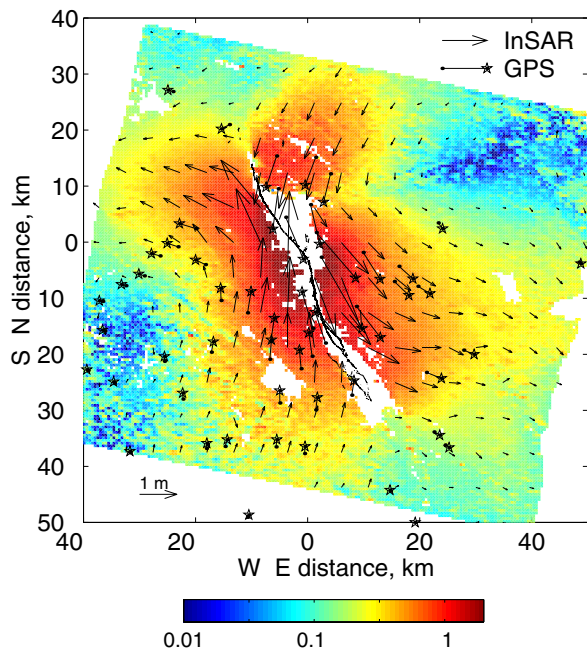
Figure 2. Coseismic horizontal displacements $\mathbf{U_h} = (U_e, U_n)$. Colors denote the horizontal displacement amplitude, $U_h = \sqrt{U_e^2 + U_n^2}$, in meters, and arrows show a sub-sampled horizontal displacement field obtained from the InSAR data. Black triangles denote survey-mode GPS stations, and starred arrows show horizontal displacement vectors inferred from the GPS data analysis (D. Agnew et al., manuscript submitted to BSSA, 2001).

can see, the decorrelated areas in general outline the surface rupture pattern. In addition to the LOS displacements, we calculate azimuthal offsets (AZO) by cross-correlating pre- and post-seismic radar amplitude pixels along the satellite track. Azimuthal offsets for the descending orbit are shown in Figure 1c. We obtain the AZO displacements only for a subset of the interferogram because of a vanishing signal-to-noise ratio beyond about 40 km from the epicenter.

The InSAR data shown in Figures 1a-c provide continuous maps of ground displacements in three different projections, which may be sufficient to retrieve three orthogonal components of the surface displacement field, $U_i(e, n)$, where $i = e, n, u$ are the basis coordinates (e.g., East, North, and Up). The measured line of sight displacements d_{los} represent a projection of the vector displacement field U_i onto the satellite look vector,

$$[U_n \sin \phi - U_e \cos \phi] \sin \lambda + U_u \cos \lambda + \delta_{los} = d_{los}, \quad (1)$$

where ϕ is the azimuth of the satellite heading vector (positive clockwise from the North), λ is the radar incidence angle at the reflection point, and δ_{los} is the measurement error (e.g., due to imprecise knowledge of satellite orbits, atmospheric delays, poor phase coherence, incorrect DEM, etc.). The azimuthal offsets d_{azo} are a projection of a horizontal component of the displacement vector onto a satellite heading vector,

$$U_n \cos \phi + U_e \sin \phi + \delta_{azo} = d_{azo}, \quad (2)$$

where δ_{azo} is the corresponding measurement error. The minimum ("intrinsic") measurement errors are of the order of a fraction of the radar wavelength for the line of sight (phase) measurements, and a fraction of the pixel size for
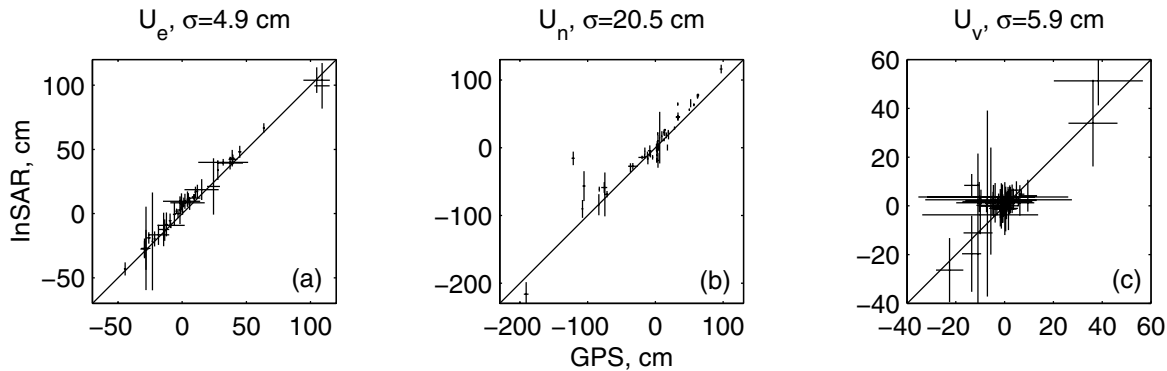
Figure 3. A comparison between the InSAR-derived co-seismic displacements and GPS observations. InSAR data represent displacements within ~500m×500m pixels that correspond to the GPS station locations. Horizontal bars show the formal errors of the GPS solutions, and vertical bars indicate errors in the InSAR AZO data inferred from pixel co-registration. σ is the rms misfit between the InSAR and GPS data for each component of the displacement vector U_i.

the azimuthal offset (amplitude) measurements. For the ERS satellites, the radar wavelength is ~5.7 cm, and the along-track pixel size is ~4 m. Therefore, the azimuthal offsets are typically much less precise than the LOS displacements, $\delta_{azo} >> \delta_{los}$. However, due to an exceptionally high correlation of the descending interferogram, the AZO errors (estimated in the process of cross-correlation) are less than 10 cm for most of the interferogram. In Figure 1c, white areas correspond to pixels having signal-to-noise ratio less than 1.5 for AZO displacements greater than 20 cm. Because both δ_{azo} and δ_{los} are expected to be small compared to co-seismic displacements in the near field of the Hector Mine earthquake, we neglect them in our analysis. To exclude possible systematic errors due to imprecise satellite orbits, we have determined orbital corrections as part of a joint inversion of the InSAR and "far field" continuous GPS data for a best-fitting deformation source (we note that the GPS data, although useful, are not essential for our orbit error estimates). After subtracting the orbital corrections, we invert the data shown in Figures 1a-c for a three-component co-seismic vector displacement field U_i. For each pixel of the InSAR image, we solve a linear system of two equations (1) for the LOS displacements from the ascending and descending orbits, and one equation (2) for the azimuthal offsets from the descending orbit. Vertical, East, and North components of the co-seismic displacement field yielded by our solution are shown in Figures 1d-f. The imaging configuration of the ERS satellites, and the orientation of the Hector Mine rupture, are such that the azimuthal offsets are mostly sensitive to the North-South displacements, while the line of sight measurements from both orbits are strongly sensitive to the vertical, modestly sensitive to East-West, and weakly sensitive to North-South displacements. Figure 2 shows the magnitude (color) and direction (arrows) of a horizontal component of the displacement field.

It is instructive to compare the three-component displacement field derived from the InSAR data with the independent survey-mode GPS data. Positions of the available GPS stations are shown in Figure 2, and Figure 3 presents a comparison of the InSAR-derived displacements with the GPS measurements. While the GPS solutions are only preliminary, and formal GPS errors are likely to underestimate the actual measurement uncertainties, the agreement between the two data sets is quite good. One notable exception is a GPS station immediately to the North-East of the epicenter, which shows a significant southward offset, while the InSAR data (dominated by the azimuthal offsets) indicate only a minor displacement (Figure 3b). We point out that the AZO data are quite noisy within a few kilometers from the earthquake epicenter, presumably due to intense ground shaking. Excluding the near-epicenter GPS stations, the rms misfit between the InSAR and GPS data is several centimeters for all three components of the displacement field. These results indicate that accurate 3-D maps of deformation due to major shallow crustal earthquakes may be produced in areas that lack ground-based observations, given sufficiently short satellite orbit repeat times, and observations from different lines of sight.

Discussion and conclusions

As one can see in Figures 1d and 2, both vertical and horizontal displacements of the Earth's surface are mostly antisymmetric with respect to the rupture plane of the Hector Mine earthquake. The inferred vertical displacements might result from a dip-slip component of the fault offset. Alternatively, displacements seen in Figure 1d may represent regions of compression (uplift) and tension (subsidence) at the edges of a strike-slip asperity in the northern part of the fault. Modeling using a steeply dipping strike-slip rectangular dislocation intersecting a free surface of an elastic half-space shows that the amplitude of vertical displacements near the edges of a dislocation is of the order of 10% of a strike-slip offset. This is similar to the relative amplitudes of vertical and horizontal displacements associated with the Hector Mine rupture (Figures 1d and 2). That most of the strike-slip motion due to the earthquake has occurred in the northern section of the fault is apparent from the horizontal displacement map (Figure 2). The maximum strike-slip offset of 5.5-6m, and gradual tapering of the surface offset toward the rupture ends suggested by the InSAR data are in excellent agreement with the field mapping results [*USGS et al.*, 2000].

Peltzer et al. [1998], using the ERS InSAR data from one look direction, inferred a significant asymmetry in the strike-slip displacements due to the 1997 M_w7.6 Manyi (Tibet) earthquake, and argued that such an asymmetry results from non-linear elastic deformation of the upper crustal

rocks. While the horizontal displacements due to the Hector Mine earthquake are predominantly antisymmetric with respect to the fault plane (Figure 2), some deviations from antisymmetry are apparent; in particular, near the southern tip of the fault, displacements on the eastern side of the fault seem to be larger than those on the western side. Such a pattern is opposite to that predicted by a non-linear elastic model, as greater displacements occur in a nominally compressional quadrant of the right-lateral Hector Mine rupture. We suggest that the observed asymmetry in strike-slip displacements may result from deviations of the earthquake rupture plane from the vertical. For a non-vertical strike-slip dislocation in an elastic half-space, surface displacements on a foot wall side of the fault decay away from the fault faster than displacements on the hanging wall side. If this mechanism is responsible for the asymmetry in displacements seen in Figure 2, our observations suggest that the southern section of the Hector Mine rupture is dipping to the East. Such a conclusion is supported by the results of a joint inversion of the space geodetic data for the fault geometry and slip distribution (unpublished results by the authors), as well as by the aftershock data (E. Hauksson, personal communication). The asymmetry in strike-slip displacements inferred from the InSAR data for the 1997 Tibet earthquake [*Peltzer et al.*, 1998] might be explained by similar along-fault changes in the dip angle. Alternatively, asymmetric LOS displacements may result from vertical deformation. Results shown in Figure 1d indicate that significant vertical displacements along major strike-slip faults (e.g., due to spatially variable strike slip) may not be unusual.

Our data lend support for observations of *Sandwell et al.* [2000], who identified shallow slip induced by the Hector Mine earthquake on neighboring faults using the LOS gradient data from the descending orbit alone. While the LOS measurements from one orbit do not allow one to distinguish between the vertical and horizontal motion, the azimuth offset data, as well as the 3-D vector displacement field inferred from our analysis indicate that the induced slip is indeed predominantly horizontal, with both right- and left-lateral sense of slip on the NW trending faults (see Figures 1c and 2). The shallow slip revealed by the InSAR data suggests that the uppermost sections of strike-slip faults may accumulate less elastic strain during the interseismic period than the deeper (locked) fault sections.

References

Fialko, Y., and M. Simons, Deformation and seismicity in the Coso geothermal area, Inyo County, California: Observations and modeling using satellite radar interferometry, *J. Geophys. Res.*, *105*, 21,781–21,793, 2000.

Fujiwara, S., T. Nishimura, M. Murakami, H. Nakagawa, M. Tobita, and P. Rosen, 2.5-D surface deformation of M6.1 earthquake near Mt Iwate detected by SAR interferometry, *Geophys. Res. Lett.*, *27*, 2049–2052, 2000.

Massonnet, D., M. Rossi, C. Carmona, F. Adragna, G. Peltzer, K. Feigl, and T. Rabaute, The displacement field of the Landers earthquake mapped by radar interferometry, *Nature*, *364*, 138–142, 1993.

Peltzer, G., F. Crampe, and G. King, Evidence of nonlinear elasticity of the crust from the M_w 7.6 Manyi (Tibet) earthquake, *Science*, *286*, 272–276, 1998.

Sandwell, D., L. Sichoix, D. Agnew, Y. Bock, and J.-B. Minster, Near real-time radar interferometry of the M_w 7.1 Hector Mine Earthquake, *Geophys. Res. Lett.*, *27*, 3101–3104, 2000.

USGS, SCEC, and the California Division of Mines & Geology, Preliminary report on the 16 October 1999 M7.1 Hector Mine, California, earthquake, *Seismol. Res. lett.*, *71*, 11–23, 2000.

Y. Fialko, D. Agnew, Institute of Geophysics and Planetary Physics, Scripps Institution of Oceanography, University of California San Diego, La Jolla, CA 92093. (e-mail: fialko @radar.ucsd.edu; dagnew@ucsd.edu)

M. Simons, Seismological Laboratory, California Institute of Technology, Pasadena, CA 91125. (e-mail: simons@ gps.caltech.edu)